HEAT TRANSFER IN THE TIP REGION OF A ROTOR BLADE SIMULATOR*

M.K. Chyu† and D.E. Metzger
Arizona State University
Tempe, Arizona

The blades of axial turbine stages rotate in close proximity to a stationary peripheral wall (sometimes termed an outer ring or stationary shroud). Differential expansion of the turbine wheel, blades, and the shroud causes variations in the size of the clearance gap between the blade tip and stationary shroud. The necessity to tolerate this differential thermal expansion dictates that the clearance gap cannot be eliminated altogether, despite accurate engine machining [1]. This gap clearance provides a narrow flow passage between the pressure and suction sides of the blade and the resulting flow passing through the passage is often referred as the "tip leakage" flow.

The tip leakage flow is detrimental to engine performance and undesirable in practical design strategies. The primary detrimental effect of tip leakage flow is the reduction of turbine stage efficiency, but the convective heat transfer associated with the flow is an important secondary effect. The surface area at the blade tip in contact with the hot working gas represents an additional thermal loading on the blade which, together with heat transfer to the suction and pressure side surface area, must be removed by the blade internal cooling flows [2,3].

Very limited information on turbine tip heat transfer and fluid flow has been reported to date, and almost all of the published work dealing with clearance gap flows involves consideration only of plain flat blade tips. However, a strategy commonly employed to reduce tip flow and heat transfer is to groove a single rectangular cavity chordwise along the blade tip. The groove acts like the cell of a labyrinth seal to increase the pressure drop and thus reduce the flow for a given pressure differential across the tip. The reduction of the flow will also act to reduce heat transfer. A schematic diagram representing the geometry of a grooved blade tip, viewed from a coordinate system fixed relative to the blade, is shown in Fig. 1. The outer shroud can be considered moving in the general direction from the suction side to the pressure side, with relative velocity equal to U_w. The leakage flow, as denoted by U in the figure, is driven by the pressure difference between two sides of the blade and flows in the direction opposite to the shroud motion. With this general configuration in mind, the grooved tip problem can be categorized as

* Work done under NASA grant NAG 3-623
† Present Address: Department of Mechanical Engineering,
Carnegie Mellon University, Pittsburgh, PA 15213

C-5

fluid flow and heat transfer over a shrouded rectangular cavity. The flow field over a cavity is characterized by flow separation and shear layer reattachment resulting in complex flow patterns with substantial effects on the friction drag and heat transfer [5-7]. Most of the previous studies on cavity problems have been considered as a flow system in which the cavity is open to a usually well-specified approaching flow over an otherwise smooth and stationary surface. The approaching flow may be a wall boundary layer for external flow or a well developed channel flow.

The grooved tip differs from the aforementioned unshrouded situation by virtue of the confined nature of the geometry as well as by the proximity of moving shroud. The degree of similarity between the heat transfer characteristics of the grooved tip and those of previous cavity studies has been unclear until recently [7-9]. The results reported in several relating studies, including the one presented earlier in the HOST program [8], have generally indicated that the characteristic of flow pattern and heat transfer in a tip region is virtually unaffected by the relative shroud movement. The nature of the shear layer separated from the sharp edge of a cavity upstream wall has predominated the transport mechanisms in a cavity so that the effect from the shroud motion becomes secondary. Consequently, the cavity shape and the gap size are the two most influential parameters. This implies that the entire tip leakage problem can be modeled in a stationary system without the shroud-moving effect.

In Ref. [8], detailed local heat transfer characteristics on all surfaces of shrouded, rectangular cavities are reported. The varying parameters include the cavity depth-to-width ratio, D/W, gap clearance-to-cavity width ratio, C/W, relative shroud moving speed, U_w/U, and Reynolds number, $Re = UC/\nu$. The naphthalene ($C_{10}H_8$) sublimation mass transfer technique in association with a computer-controlled, automated surface contouring measurement system is employed. This experimental system provides better control and high data accuracy for a local study. The mass transfer results can be transformed into their counterparts in heat transfer by invoking an analogy between these two transfer processes [10,11].

This paper, an extension to Ref. [8], describes the updated development of the project currently being conducted at Arizona State University. It consists of two major parts. First is the continuing measurement effort of the mass transfer from cavities, with an emphasis on the effect of cavity orientations relative to the main flow direction. The second part is a finite-difference computation for turbulent air flow and heat transfer over a two-dimensional, shrouded, rectangular cavity. This is intended to numerically model the experimental system studied in Ref. [8], and the fundamental aspects of the cavity problem, as reflected in the measured data, can thus be understood.

EXPERIMENTAL STUDY

Objectives and Despcription of Model

To gain a detailed understanding of the heat transfer fundamentals

in a complex separated-flow system and to provide turbine manufacturers with design information, it is desirable to model the grooved tip by using a cavity with an actual blade airfoil shape. Fig. 2 shows a typical blade shape and grooved configuration for a low-aspect-ratio, small/medium size engine in which tip leakage is a critical problem. In this case, the pressure differential across the tip leakage-passage is non-uniform along the chordwise direction. Thus the leakage flow may have an angle-of-attack to the tip groove different from that of a normally positioned cavity. This also implies that the flow separates from a sharp edge which is not perpendicular to the flow mainstream direction. The flow is more complex than that of a normally positioned cavity and involves heat transfer with three-dimensional, separated shear flow. It is speculated that vortices with different orientations and strength may exist in the cavity, and that the vortices rotate in a helical fashion creating wavy characteristics in both the flow field and the heat transfer.

As a preliminary study to the tip cavity with an actual blade shape, the present work emphasizes on determining the effect of the flow angle-of-attack on the cavity heat transfer. This is facilitated by placing a rectangular cavity with its two parallel side walls inclined to the flow mainstream direction, as shown in Fig. 3. For a fixed flow direction, the term "skewed cavity" can thus be used to describe this geometry. The degree of cavity skewness is represented by the magnitude of θ as defined in Fig. 3. In the present study, θ varies between 90° and 75° ($\theta = 90^\circ$, 85°, 80° and 75°), where $\theta = 90^\circ$ represents the case without skewness generally referred to be the rectangular cavity in the literature and used in Ref. [8]. Along the cavity spanwise direction (Z-axis in Fig. 3), the skewness can produce pressure gradients and flow components which in general are either nonexistent or insignificant in a normally positioned, two-dimensional cavity. Although a thorough understanding of the transport mechanism associated with this phenomena is lacking, experimental data from previous studies of heat transfer enhancement have indicated that a skewed flow-separation can result in a higher heat transfer than its unskewed counterpart [12], provided that the skewed flow-separation is sufficiently strong. In the present application, the degree of skewness is moderate. It is intended to investigate the effect of θ variation on the heat transfer in a skewed cavity as compared to its unskewed counterpart. The comparison will help to assess the utility of results from the rectangular cavity experiments, e.g. Ref. [8], in predicting heat transfer in the more complex cavities existing on actual turbine blades. In addition to θ variation, four different cavity depth-to-width ratios, $D/W = 0.9$, 0.45, 0.23, and 0.15, are tested for each θ .

To isolate the primary effect of interest, no attempt is made to model the detailed, complex leakage flow field as it exists with the actual blade shape. Since the shroud effect, especially the movement relative to the cavity, is considered to be unimportant in most of the turbine applications, it is excluded in the present test. However, a comparison between the present results and those from studies with shroud or confined cavities [7,8] will be made, so that the influence of shroud presence on the heat transfer in a cavity can be understood.

Experimental System

The naphthalene ($C_{10}H_8$) sublimation mass transfer technique is employed herein. The subliming mass transfer process takes place when the solidified naphthalene is exposed to the air stream in a tunnel. The local mass transfer coefficient at a certain location can be inferred from the depth change of naphthalene at this location before and after a test run. A computer-controlled, automated surface profile measurement system had been developed earlier for this project, which provides high data accuracy and operational convenience. The mass transfer results can be transformed into their counterparts in heat transfer by invoking an analogy between these two transfer processes. Details on the measurement system and analogy has already been discussed in Ref. [8,11].

A specially designed open-circuit wind tunnel, approximately 4.5 meters in total length, is used for the present study. Air is drawn from a 100 HP compressor into the tunnel, passing a series of screen pads before reaching the test section. The test section, located approximately 0.9 meter upstream of the tunnel exit, has a uniform cross-section of 101 mm high by 152 mm wide. The side walls are made of acrylic plastic (Plexiglas) with a thickness of 19 mm. The framework of cavities being tested is made of aluminum tooling plate. Details of the cavity geometry are shown in Fig. 3. The shaded region shown in the figure represents the mass transfer active area where the surface is coated with naphthalene. The naphthalene covered cavity is inserted into the test section of the wind tunnel and tightened by screws against the tunnel floor.

Depths of the cavity walls are physically identical for all the cases, D = 5.72 mm (0.225"). The effective cavity span across the tunnel is maintained at 152 mm (6.0") which is equivalent to approximately 26 times the cavity depth. For cavities with $\theta = 90^\circ$, this high span/depth ratio tends to result in a generally two-dimensional separated flow and mass transfer. The mass transfer measurements in this study are made covering the entire cavity, with the number of measured data points increasing with the size of mass transfer active area. Approximately 200 data points are measured for D/W = 0.9 and 800 points for D/W = 0.15. For a given value of a cavity aspect ratio, the naphthalene coated area increases with an increase in cavity skewness, as shown in Figure 3.

The measured velocity profile at the location of the naphthalene leading edge reveals characteristics of a fully turbulent boundary layer, and the boundary layer thickness (0.99 U) thickness at that location is 11 mm ($\approx 1.9D$). The Reynolds number based on the cavity depth and U is about 1.76×10^3.

Results and Discussion

Most of the mass transfer results are presented in terms of the Stanton number, $St = h_m/U$, where h_m is the mass transfer coefficient. For a comparison purpose, the mass transfer measurements have been made on a flat naphthalene plate without a cavity in the same tunnel operating with the same flow conditions and $\theta = 90^\circ$. The local Stanton

number shows a power law dependency on the streamwise coordinate (X_n/D) of the type 4.19×10^{-3} $(X_n/D)^{-0.23}$, where X_n is the streamwise distance from the mean starting point of mass transfer (see Fig. 1). Based on this equation, the area-averaged Stanton numbers are 3.24, 3.03, 2.76 and 2.58×10^{-3} for the same streamwise distance as that for an unskewed cavity with D/W = 0.9, 0.45, 0.23 and 0.15, respectively. The equation compares favorably with correlations [13] for heat transfer from a flat plate to a turbulent boundary layer with a zero freestream pressure gradient, although the absolute values of Stanton numbers are somewhat different. This is believed to be due partially to the inactive mass transfer starting length. The agreement provides confidence in the present mass transfer technique as well as in the measurement system. The uncertainty in the local Stanton number, based on the methods of Ref. [14], is estimated to be approximately 10%. The repeatability of all the present tests is within 5%.

Local mass transfer results are shown in Figs. 4 to 6. The open symbols represent the measured data for different values of θ along the center-line of test section (Z/D = 0). It is expected that the asymmetric mass transfer behavior exists across the cavity span (Z direction), at least for $\theta \neq 90^{\circ}$. However, the data measured within the domain $|Z/D| \leq 9.0$ is quite scattering and no clear trend or correlation between St and Z/D can be found. Thus, in addition to the center-line data, the range of the corresponding data over the entire measurement domain is given as a shaded region on each figure. The aforementioned effect is likely due to the relatively moderate degree of skewness coupling with the complex separated flow field and transfer mechanism and different cavity geometries. This is also supported by an auxiliary study using the graphite-oil technique to visualize the flow streak line on a cavity floor. An inclined, distorted flow separation-reattachment line on a cavity floor can only be seen when $D/W \leq 0.1$ and $\theta \leq 60^{\circ}$. For all the cases tested in the present mass transfer study, a wavy flow motion has been observed across the cavity span. The motion, having an amplitude in the order of cavity width, appears to be stronger near the central region (Z/D = 0) and with a higher degree of cavity skewness. This phenomena is also observed in the previous studies dealing with rectangular cavities with normal flow angle-of-attack [15]. The wavy motion, at least in part, may be responsible for the data variation along the Z direction.

Figure 4 shows the distribution of local St on the cavity floor and surfaces upstream and downstream of the cavity. The streamwise coordinate in these figures is normalized by the cavity height, D. The mass transfer variation with X/D is similar for the different values of D/W. The mass transfer coefficient is generally low near the front corner of the cavity and increases with X/D to reach a maximum. This is followed by a decrease toward the downstream wall. The magnitude of this maximum has the lowest value for D/W = 0.9 and the highest for D/W = 0.23, and its location moves downstream as the width of the cavity increases. The increase of mass transfer with X/D in the front portion of the cavity is characteristic of a separated boundary layer from a sharp-edged, downstream-facing step. For a normally positioned cavity, a recirculating region is formed immediately downstream of the step, and it is followed by a reattachment zone if no downstream wall (the upstream-facing wall) is present or if the cavity aspect ratio, D/W, is

low. For cavities with a medium/small value of the aspect ratio, e.g. $0.2 \leq D/W \leq 1$, an elliptic vortex is formed as a result of a part of the separated shear layer impinging on the cavity downstream wall and then flowing toward the cavity floor [5]. The resulting vortex fills the entire cavity. In addition, a very unsteady, small, but high-strength vortex is found near the lower corner immediately ahead of the downstream wall. High turbulence may be induced by this vortex, increasing the heat or mass transfer in the region. To a certain extent, the vortex structure is expected to be affected by the cavity-skew. The wide scattering of data near the cavity downstream corner, in particular for $D/W = 0.23$, could be caused by these reasons. The overall trend of the mass transfer distributions on the cavity floor shown in Fig. 4 agrees very favorably with previous studies for normally positioned cavities [6-8].

A distinct mass transfer characteristic on the floor is observed for $D/W = 0.45$. An additional, but rather moderate, local maximum of St occurs at $X/D = 0.5$, which is followed by a local minimum near the mid-point of the cavity floor. Similar behavior is also observed in Ref. [6,8]. According to a flow visualization study [5], for D/W approximately equal to 0.5, a stagnant region of a weak recirculation behind the cavity upstream wall is observed in addition to the primary vortex. This may account for the peculiar mass transfer distribution on the cavity floor for $D/W = 0.45$. To be noted is that, for cavities confined by a shroud as studied in Ref. [8], this peculiar mass transfer distribution occurs at $D/W = 1.0$, not $D/W \approx 0.5$. This may be attributed to the fact that the presence of shroud causes the shear-layer reattachment effect to persist in deeper cavities as compared to the cases without shroud present. In general, the characteristics of flow and heat transfer in an unshrouded cavity are corresponding to those in a shrouded cavity with a higher value of D/W.

Mass transfer measurements have also been made on the naphthalene surfaces extending one cavity depth (1D) upstream and downstream of a cavity. For a normally positioned cavity, mass transfer from the surface upstream of the cavity behaves similar to that of a flat surface with a developing boundary layer, and it is virtually unaffected by the presence of the cavity [6]. Nevertheless, this is different if the actual inlet condition of leakage flow is of concern. The sharp-edge inlet effect produces a recirculating bubble, or the vena-contracta, at the entrance region of the leakage passage. The resulting heat or mass transfer distribution in the region is characterized with a local maximum in the mid-portion of the surface, as shown in Ref. [8]. In this study, the mass transfer coefficient is very high at the leading edge of the surface and decreases with a downstream position. The effect of the θ variation on the St appears to be stronger for a larger value of D/W, as is also the range of data across the cavity span.

As a contrast to the surface upstream of a cavity, the mass transfer from the surface downstream of a cavity is dependent on the cavity width. A cavity with a small value of D/W permits the shear layer originating from the cavity upstream wall to grow thicker and to generate more turbulence in the layer before it impinges the cavity downstream wall. At least part of this highly turbulent layer may be

deflected toward the cavity top gaining a velocity component normal to the mainstream direction after the impingement. This is due mainly to the pressure difference between the region of impingement and the mainstream. For D/W = 0.15, the local maximum of St near the mid-point of the surface downstream of the cavity is believed to be due to the effect of the deflected shear-layer reattachment. This is often observed in a flow system with a sharp-edge boundary layer development. For D/W $\geq$ 0.23, this reattachment effect becomes insignificant or even non-existent and a thin separated shear layer bridges the entire cavity. The external flow would skim past the cavity without a strong interaction with the flow inside. As a consequence, the behavior of mass transfer downstream of a large D/W cavity can primarily be determined by the characteristics of the mainstream flow. The mass transfer characteristic is similar to that of a new developing boundary layer.

Figure 5 shows the local mass transfer distributions along the upstream side-wall of the cavity, i.e. the downstream-facing wall. The mass transfer from the upstream wall seems to be dominated by the vortex attached behind the wall, and it is generally lower than that of other portions of the cavity. For D/W = 0.9, the stagnant flow motion in the vortex induces a local minimum of the mass transfer coefficient at Y/D $\cong$ 0.7. For D/W $\leq$ 0.45, the mass transfer distributions are very similar; the lowest mass transfer coefficient occurs near the lower corner while the highest occurs near the top of the wall. This implies the mass transfer behavior on a cavity upstream wall may be unaffected by the aspect ratio of the cavity. The variation of St with θ is about the same along the center line for all the values of D/W tested. However, the range of St across the cavity span appears to be stronger for D/W = 0.45. This is expected to be caused by the secondary vortex existing near the front corner of the cavity, as previously discussed.

Local mass transfer distribution on the cavity downstream wall (the upstream-facing wall) is shown in Fig. 6. The fundamental mode of mass transfer mechanism for the upstream-facing wall is the impingement of the shear layer on the wall, and it generally results in a higher mass transfer coefficient as compared to a downstream-facing wall. The local St increases almost linearly with Y/D. D/W = 0.45 has the highest variation range of St across the cavity span, as it does with the mass transfer of the upstream side wall. A comparison with the results in Ref. [8] reveals that the shroud effect is insignificant on the mass transfer from the cavity side walls.

The value of the mass transfer averaged over an area is obtained by numerical integration. Fig 7 shows the area-averaged Stanton number ($\overline{St}$, left-ordinate) and the normalized overall mass transfer rate (right-ordinate) for the entire cavity. Since the variation of $\overline{St}$ vs θ is near the range of estimated experimental uncertainty, a data bar is used to represent the $\overline{St}$ for all the values of θ at a certain aspect ratio of the cavity. As shown in Fig. 7, D/W = 0.23 has the highest value of $\overline{St}$ and D/W = 0.9 has the lowest. For D/W $\geq$ 0.23, $\overline{St}$ decreases with an increase in the value of D/W. This implies that, in general, a deeper groove results in a lower heat transfer coefficient.

In the literature, the average heat transfer coefficient on the cavity floor has commonly correlated between the average Nusselt number, the Reynolds number and the cavity aspect ratio. A power correlation reported in Ref. [5] has suggested that, for $D/W \leq 0.12$, $\overline{St}$ increases as the aspect ratio (D/W) increases. However, the present results show that the opposite trend exist when $D/W \geq 0.23$; $\overline{St}$ decreases with an increase of D/W. Similar results have been reported in Ref. [6]. As a result, the cavity heat transfer within the present range of D/W is unable to be presented by a single correlation. In addition, the overall trend of average Stanton number is unaffected by the variation of cavity-skew at least within the present studying range, as shown in Fig. 7.

If the overall heat transfer rate is the major concern, the additional heat transfer area due to an increase in cavity depth becomes an important factor. The results shown in Fig. 7 indicates that, despite the lower mass transfer coefficient, the deeper cavities experience higher overall mass transfer rate than the shallower ones. This result agrees favorably with those from Ref. [7,8]. It is suggested in Ref. [7] that to groove a blade tip having a cavity with $D/W \geq 0.5$ may be undesirable.

NUMERICAL COMPUTATION

As previously mentioned, numerical computation is attempted to simulate the flow field and heat transfer near a grooved tip. The problem is modeled as the turbulent air flow over a two-dimensional, rectangular, shrouded cavity. A control-volume based finite-difference method is employed for solving a system of partial differential equations describing the conservation of mass, momentum, energy and turbulent flowfields. The formulation entails an elliptic system of equations for properly describing the separated, recirculating flow. The computer program uses the SIMPLER algorithm [16] to explicitly solve for the velocity and pressure fields. The turbulent parameters are determined by a low-Reynolds-number, k-ε model developed by Jones and Lauder [17]. The model is capable of describing the boundary layer laminarization and the boundary conditions explicitly, which is considered to be important for the present application. The momentum, continuity, and turbulence equations, together with their coupling characteristics, constitute five equations to be solved simultaneously for the converged velocity field. This is followed by the separate solution for the energy equation. For a computational domain similar to Fig. 1, the computation uses a 40 x 26 grid for all cases studied and a non-uniform spacing with dense placement near solid walls. A typical run on an IBM 3081 mainframe computer takes approximately 400 iterative steps for a converged velocity field, and an additional 30 steps are required for the temperature computation.

Fig. 8 shows a sample result of computed mean-flow pattern in a cavity with $C/W = 0.1$, $D/W = 1.0$ and $Re_c = 2 \times 10^4$. For a cavity having aspect ratio near unity, it is typical for a recirculating bubble to fill the entire cavity, and the separated shear layer to partially impinge the downstream side wall. The results compare favorably with a similar study using a high-Reynolds-number, k-ε turbulence model [9]. In Ref. [9], the inlet condition is specified at the leading edge of

the surface upstream of a cavity, and a uniform velocity profile at this location is assumed. As a result, the effect of recirculation, or vena contracta, near the gap sharp-entrance region disappears. It is argued that the transport mechanism in a cavity is largely determined by the characteristics of the shear layer separated at the sharp-edge of the upstream side wall. A perfect modeling of the inlet velocity profile may not be critical, particularly if the heat transfer inside the cavity is the major concern. This inlet condition problem is remedied in the present computation by extending the flow inlet condition further upstream from the actual gap entrance. The lower left corner in Fig. 8, denoted by i-i', is where the flow inlet condition is specified, and a uniform mean flow profile with a 10% turbulence intensity is assumed. The sharp-edge entrance effect is thus revealed and, as a result, a recirculation exists near the front portion of the gap.

Heat transfer results from the present computation are compared with the data measured in Ref. [8]. Fig. 9 shows two samples of comparison, D/W = 0.1 and 0.5 (with C/W = 0.14, $Re_c = 2.0 \times 10^4$ being the same for both), for heat transfer on the cavity floor and the surfaces upstream and downstream of the cavity. The agreement in general is very favorable, in particular for the cavity with a small value of D/W. The effect of recirculation and reattachment near the gap entrance results in a local maximum of heat transfer in the mid-portion of the surface upstream of the cavity.

CONCLUDING REMARKS

The ongoing study of heat transfer in the blade tip region emphasizes on the acquisition of detailed local information in cavities with an actual blade shape. One of the distinct characteristics involved is that the flow separates skewedly from a sharp edge which is not normal to the main flow direction. As a preliminary study to the measurement with an actual blade, this effect is investigated experimentally by performing mass transfer measurements on rectangular cavities with different flow angles-of-attack. For a moderate range of angle variation, which is typical to most turbine applications, the average heat transfer in a skewed cavity is agreeable to that in a normally positioned cavity to approximately 10%. The characteristic local heat transfer distribution is found to be mainly dependent on the cavity aspect ratio rather than the flow angle-of-attack. This implies, to a certain extent, that the utility of results from the normally positioned, rectangular cavity for predicting heat transfer in the more complex cavities used on actual turbine blades is appropriate. Additional work reported is a numerical computation of the heat transfer and fluid flow in shrouded cavities. A computer code with a finite-difference method and a low-Reynolds-number, k-ϵ turbulence model is developed for this modeling. The results compare favorably with the measurements obtained previously for this project.

REFERENCES

1. Hennecke, D.K., "Heat Transfer Problems in Aero-Engines," Heat and Mass Transfer in Rotating Machinery, D.E. Metzger and N.H. Afgan, eds. Hemisphere, Washington, D.C., 1984, pp. 353-379.

2. Metzger, D.E. and Mayle, R.E., "Heat Transfer Gas Turbine Engines," Mech. Eng., 105, No. 6, June 1983, pp. 44-52.

3. Mayle, R.E. and Metzger, D.E., "Heat Transfer at the Tip of an Unshrouded Turbine Blade," 7th International Heat Transfer Conference, Munich, 3, 192, pp. 87-92.

4. Aung, W., "Separated Force Convection," Keynote Paper, ASME/JSME Thermal Eng. Conf., Honolulu, March 20-24, 1983.

5. Yamamoto, H., Seki, N. and Fukusako, S., "Forced Convection Heat Transfer on Heated Bottom Surface of a Cavity," J. Heat Transfer, 101, 1979, pp. 475-479.

6. Chyu, M.K. and Goldstein, R.J., "Local Mass Transfer in Rectangular Cavities with Separated Turbulent Flow," Heat Transfer 1986, 3, pp. 1065-1070, Hemisphere Publication, 1986.

7. Metzger, D.E. and Bunker, R.S., "Cavity Heat Transfer on a Grooved Wall in a Narrow Flow Channel," ASME Paper 85-HT-57, 1985.

8. Chyu, M.K., Moon, H.K. and Metzger, D.E., "Heat Transfer in the Tip Region of a Rotor Blade Simulator," NASA-Lewis 5th Host Workshop, Cleveland, Oct. 21-22, 1986.

9. Chyu, M.K., Metzger, D.E. and Hwan, C.L., "Heat Transfer in Shrouded Rectangular Cavities," J. Thermophysical and Heat Transfer, 1, 1987, pp. 247-252.

10. Eckert, E.R.G., "Analogies to Heat Transfer Processes," Measurements in Heat Transfer, ed. by Eckert, E.R.G. and Goldstein, R.J., Hemisphere Publication, Washington D.C., 1976.

11. Goldstein, R.J., Chyu, M.K. and Hain, R.C., "Measurement of Local Mass Transfer on a Surface in the Region of the Base of a Protruding Cylinder with a Computer-Controlled Data Acquisition System," Int. J. Heat and Mass Transfer, 28, 1985, pp. 977-985.

12. Han J.C., Glicksman, L.R. and Rohsenow, W.M., "An Investigation of Heat Transfer and Friction for Rib-Roughened Surfaces," Int. J. Heat and Mass Transfer, 21, 1978, pp. 1143-1156.

13. Reynolds, W.C., Kays, W.M. and Kline, S.J., "Heat Transfer in the Turbulent Incompressible Boundary Layer I - Constant Wall Temperature," NASA Memo. 12-1-58W, 1958.

14. Kline, S.J. and McClintock, F.A., "Describing Uncertainties in Single Sample Experiments," Mechanical Engineering, 75, January, 1953.

15. Maull, D.J. and East, L.F., "Three-Dimensional Flow in Cavities," J. Fluid Mechanics, 16, 1963, pp. 620-632.

16. Patankar, S.V., Numerical Heat Transfer and Fluid Flow, Hemisphere Publication, 1980.

17. Jones, W.P. and Launder, B.E., "The Prediction of Laminarization with a Two-Equation Model of Turbulence," Int. J. Heat and Mass Transfer, 15, 1972, pp. 301-303.

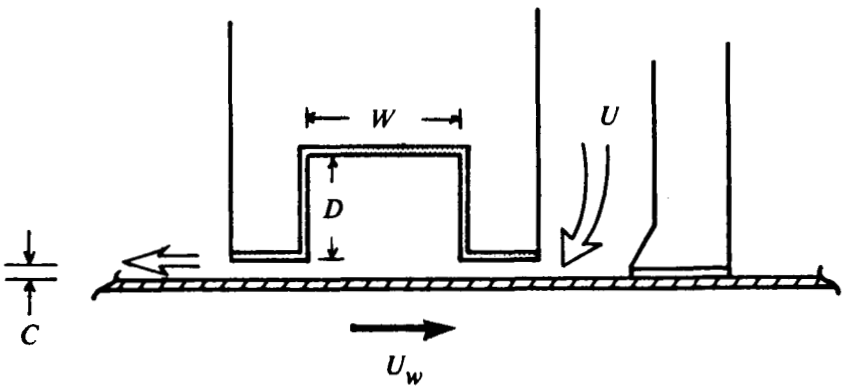

FIGURE 1. Schematic View of Shrouded Cavity

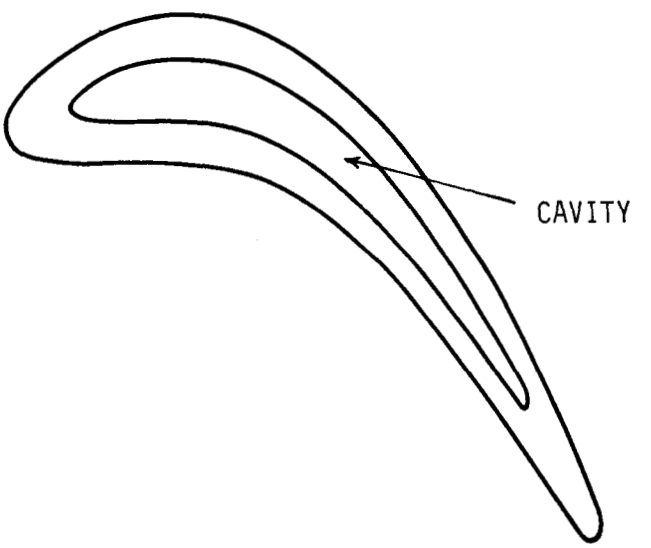

FIGURE 2. Cavity with Actual Blade Shape

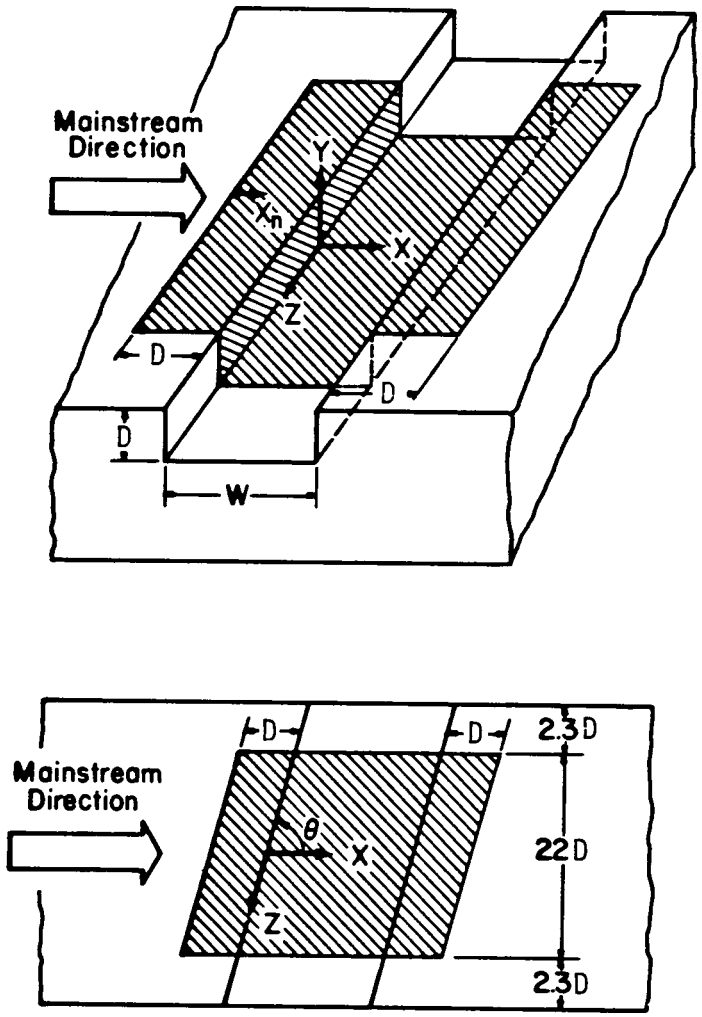

(Top View)

FIGURE 3. Skewed Rectangular Cavity

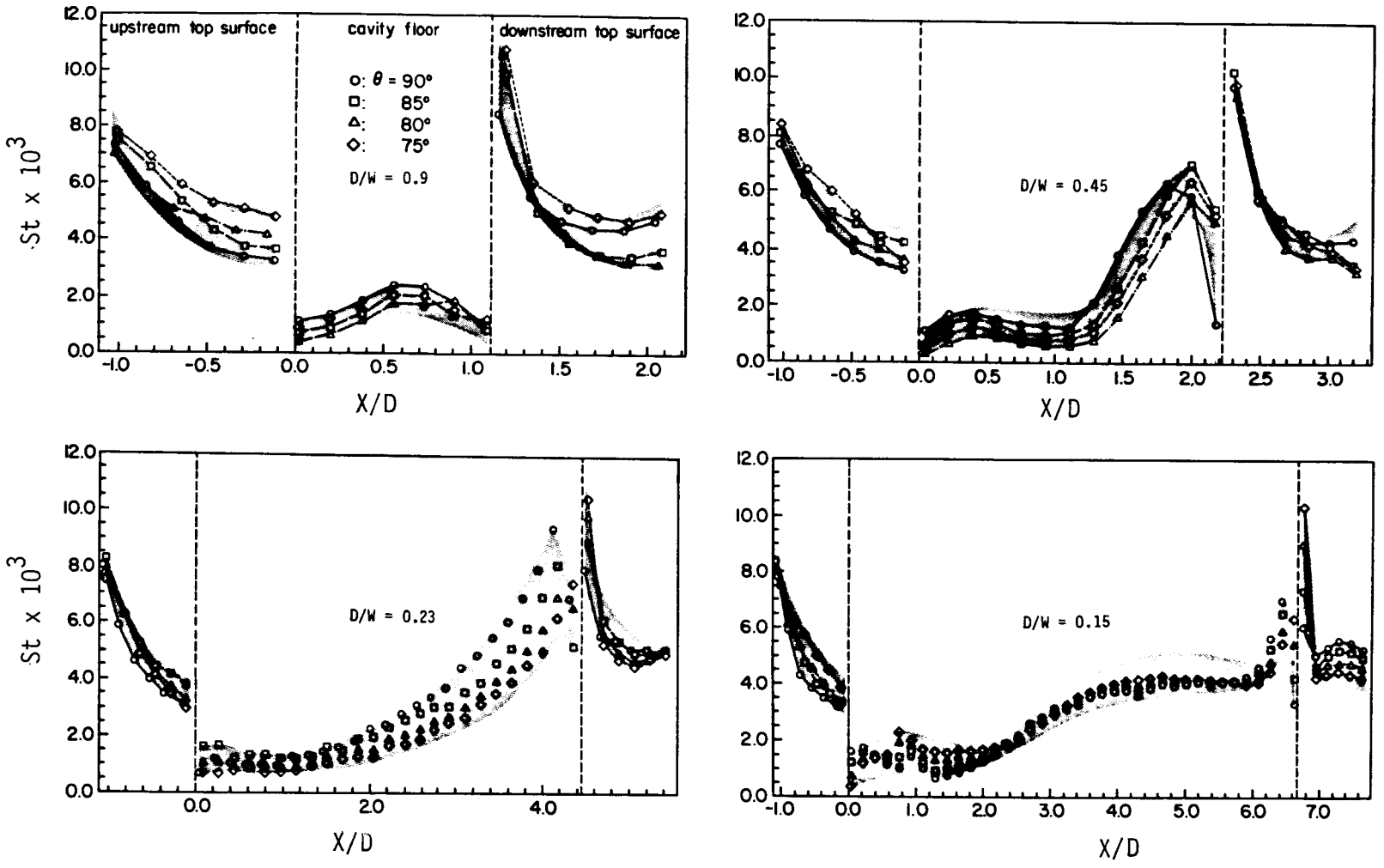

FIGURE 4. Local Mass Transfer Distribution on Cavity Floor and Surfaces Upstream and Downstream of Cavity, (Z/D = 0)

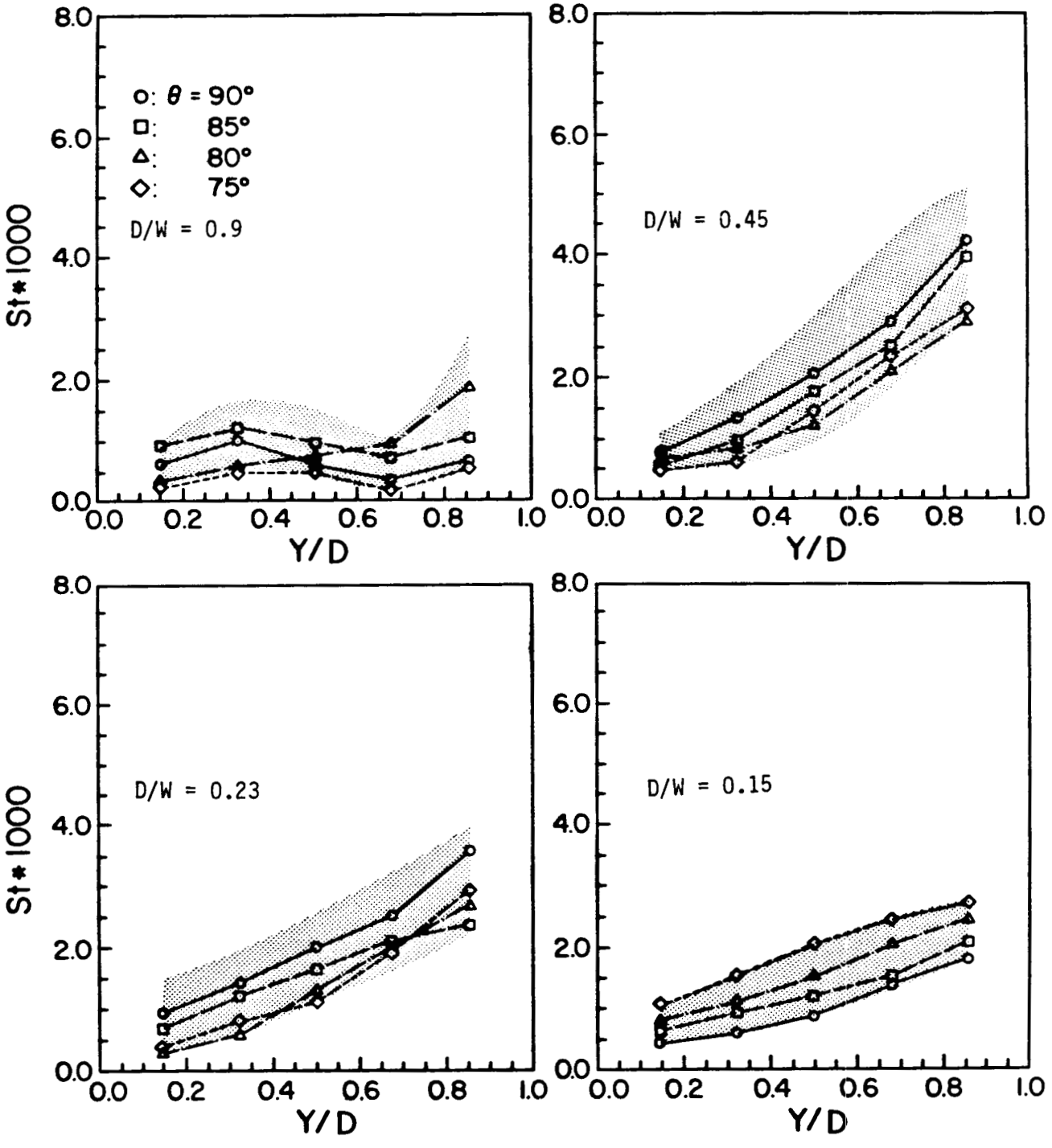

FIGURE 5. Local Mass Transfer Distribution on Cavity Upstream Side-Wall, (Z/D = 0)

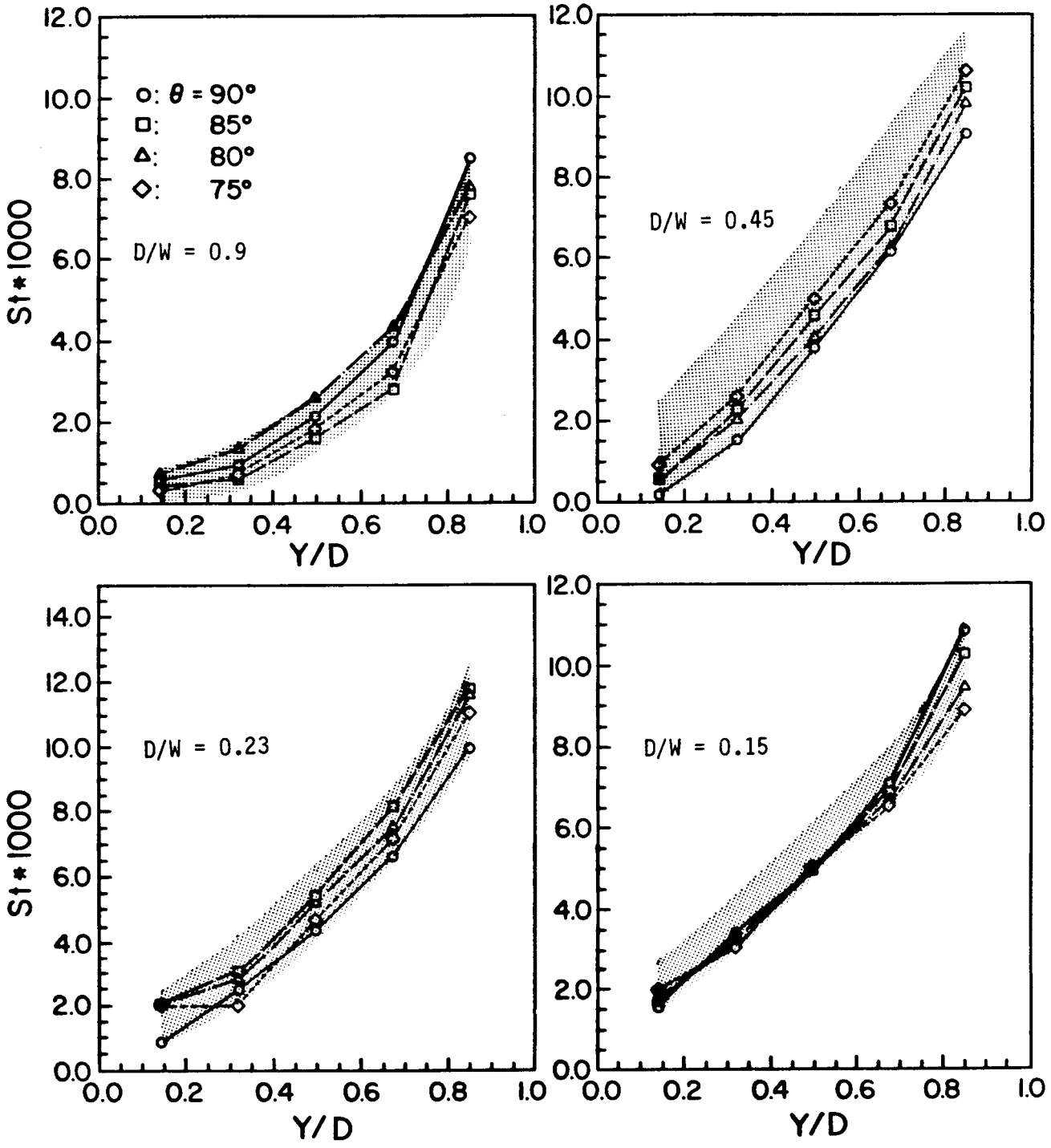

FIGURE 6. Local Mass Transfer Distribution on Cavity Downstream Side-Wall, (Z/D = 0)

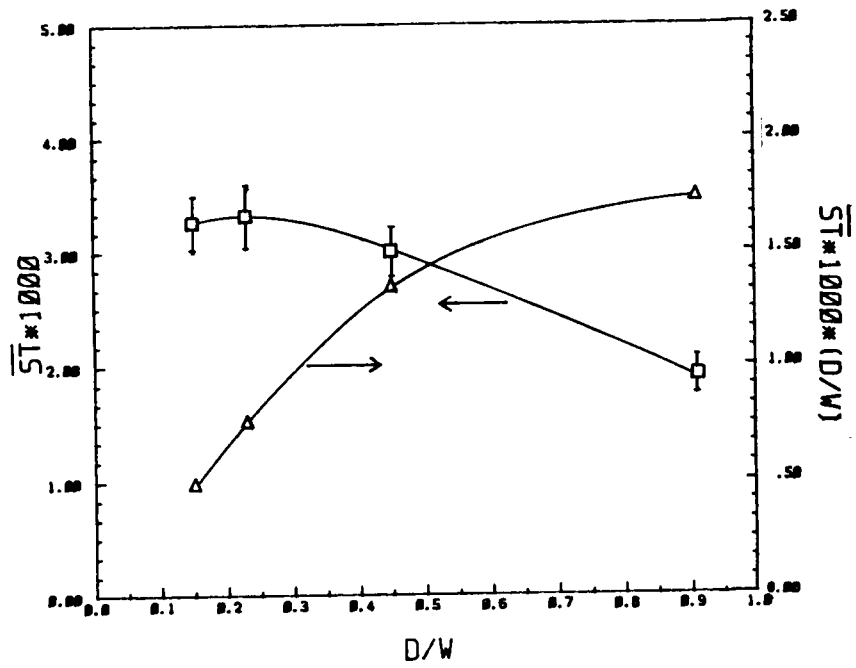

FIGURE 7. Area-Averaged Mass Transfer

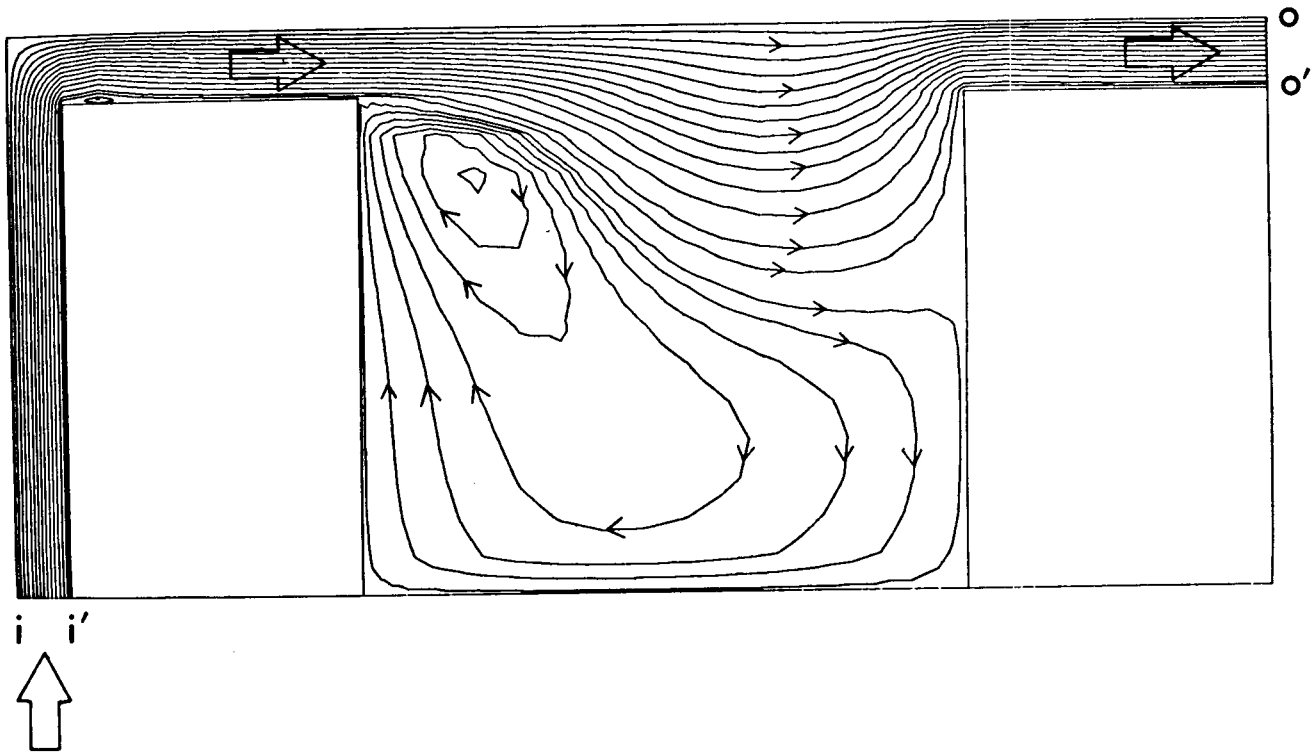

FIGURE 8. Computed Streamline Pattern;
C/W = 0.1, D/W = 1.0, Re_c = 2.0 x 10^4.

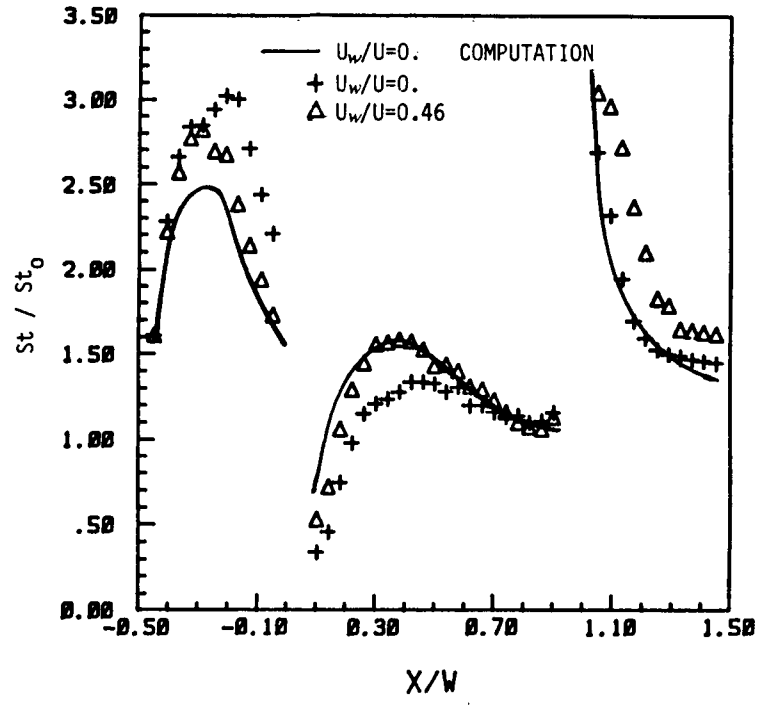

(a). D/W = 0.1

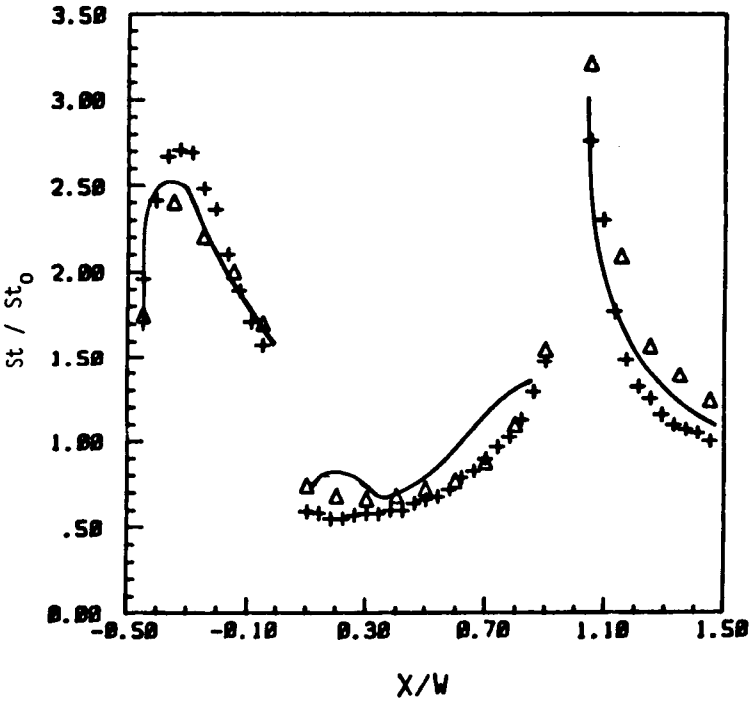

(b). D/W = 0.5

FIGURE 9 Local Mass Transfer; C/W = 0.14, Re_c = 2.0 x 10^4